Please cite the Published Version

Title:

Unveiling the tyrosinase inhibitory potential of phenolics from *Centaurium*

***spicatum*: bridging *in silico* and *in vitro* perspectives**

Authors and affiliations:

Reem S. Alruhaimi[1], Ayman M. Mahmoud[2]*, Ibrahim Elbagory[3], Ahmad F.

Ahmeda[4,5], Ashraf A. El-Bassuony[6], Al Mokhtar Lamsabhi[7,8], Emadeldin M.

Kamel[6]

[1]Department of Biology, College of Science, Princess Nourah bint Abdulrahman University, Riyadh 11671, Saudi Arabia.
[2]Department of Life Sciences, Faculty of Science and Engineering, Manchester Metropolitan University, Manchester M1 5GD, UK.
[3]Department of Pharmaceutics, Faculty of Pharmacy, Northern Border University, Rafha 76321, Saudi Arabia.
[4]Department of Basic Medical Sciences, College of Medicine, Ajman University, Ajman 346, United Arab Emirates.
[5]Center of Medical and Bio-allied Health Sciences Research, Ajman University, Ajman 346, United Arab Emirates
[6]Organic Chemistry Department, Faculty of Science, Beni-Suef University, Beni-Suef 62514, Egypt.
[7]Departamento de Química, Módulo 13, Universidad Autónoma de Madrid, Campus de Excelencia UAM-CSIC Cantoblanco, Madrid 28049, Spain.
[8]Institute for Advanced Research in Chemical Sciences (IAdChem), Universidad Autónoma de Madrid, Madrid 28049, Spain.

*Corresponding author:
Ayman M. Mahmoud
Department of Life Sciences, Faculty of Science and Engineering, Manchester Metropolitan University, Manchester M1 5GD, UK
ORCID ID: 0000-0003-0279-6500
E-mail: a.mahmoud@mmu.ac.uk

Abstract

Phenolics, abundant in plants, constitute a significant portion of phytoconstituents consumed in the human diet. The phytochemical screening of the aerial parts of *Centaurium spicatum* led to the isolation of five phenolics. The anti-tyrosinase activities of isolated compounds were assessed through a combination of *in vitro* experiments and multiple *in silico* approaches. Docking and molecular dynamics (MD) simulation techniques were utilized to figure out the binding interactions of isolated phytochemicals with tyrosinase. The findings from molecular docking analysis revealed that isolated phenolics were able to bind effectively to tyrosinase and potentially inhibit substrate binding, consequently diminishing the catalytic activity of tyrosinase. Among isolated compounds, cichoric acid displayed the lowest binding affinity and the highest extent of polar interactions with the target enzyme. Analysis of MD simulation trajectories indicated that equilibrium was reached within 30 ns for all complexes of tyrosinase with the isolated phenolics. Among the five ligands studied, cichoric acid exhibited the lowest interaction energies, rendering its complex with tyrosinase the most stable. Considering these collective findings, cichoric acid emerges as a promising candidate for the design and development of a potential tyrosinase inhibitor. Furthermore, the *in vitro* anti-tyrosinase activity assay unveiled significant variations among the isolated compounds. Notably, cichoric acid exhibited the most potent inhibitory effect, as evidenced by the lowest IC_{50} value (7.92 ± 1.32 µg/ml), followed by isorhamnetin and gentiopicrin. In contrast, sinapic acid demonstrated the least inhibitory activity against tyrosinase, with the highest IC_{50} value. Moreover, cichoric acid exhibited a mixed inhibition mode against the hydrolysis of L-DOPA catalyzed by tyrosinase, with K_i value of 1.64. Remarkably, these experimental

findings align well with the outcomes of docking and MD simulations, underscoring the consistency and reliability of our computational predictions with the actual inhibitory potential observed *in vitro*.

Keywords

Tyrosinase, *Centaurium spicatum*, Molecular docking, Molecular dynamics simulations, Phenolic compounds.

1. Introduction

Tyrosinase, a copper-containing enzyme, plays a pivotal role in melanin biosynthesis and its implications in various physiological pathways, such as skin pigmentation, wound healing, and immune responses to pathogens [1]. The intricate structure of tyrosinase enables precise tyrosine recognition and binding, and the catalytic activity drives the conversion of tyrosine into melanin, essential for skin pigmentation and protection [2]. Tyrosinase is responsible for synthesizing melanin, a pigment that serves to shield the skin from ultraviolet radiation [3]. Nonetheless, dysregulation of tyrosinase activity and excessive melanin production and deposition can lead to conditions such as hyperpigmentation and skin melanoma [3]. Consequently, tyrosinase inhibitors are frequently employed in many fields such as dermatology, cosmetics, and pharmaceuticals because of their efficacy in regulating skin-related conditions such as hyperpigmentation [4]. Natural tyrosinase inhibitors are often preferred over their synthetic counterparts due to the potential adverse effects associated with the latter, such as skin irritation, allergic reactions, and other undesirable responses [5].

Centaurium spicatum (*C. spicatum*), a member of the *Gentianaceae* family, is known for its high extent of chemical constituents and diverse pharmacological applications [6]. *C.*

spicatum contains a plethora of bioactive secondary metabolites, including iridoids, flavonoids, phenolic acids, and terpenoids, among others [6]. These bioactive phytoconstituents contribute significantly to the various biological activities of this species, including antioxidant, anti-inflammatory, antimicrobial, antidiabetic, and hepatoprotective activities [6-9]. Moreover, *C. spicatum* has been traditionally employed in folk medicine for the therapeutic remedies of digestive upset, liver diseases, fever, and wounds [10]. Thus, the diverse chemical constituents found in *C. spicatum* highlight its extensive range of biological activities and indicate its significance as a valuable reservoir of natural remedies and therapeutic agents.

The integration of computational tools such as docking and molecular dynamics (MD) simulations has gained significant attention in the realm of drug discovery and development, offering substantial outcomes [11]. Molecular docking provides valuable insights for the foretelling of the binding affinities and orientation of drugs in the binding pocket of target proteins and enzymes [12]. The outcomes of molecular docking analyses offer valuable information for the drug-protein interactions [13]. On the other hand, MD is an important technique for exploring the temporal evolution and stability of protein-ligand complexes, thereby yielding key insights into structural and functional dynamics [14]. This computational tool allows for a deep figuring out of the dynamic profile and resilience of these complexes, leading to a comprehensive exploration of their complex attribute [15]. In this study, we adopted a combination of both *in silico* and *in vitro* approaches to study the efficacy of phenolic compounds isolated from *C. spicatum* as inhibitors of tyrosinase. Through docking virtual screening, we aimed to forecast binding modes and free energies of the isolated phenolics to the active site of tyrosinase. Additionally, the dynamic behavior

4

of various isolated phenolics-tyrosinase complexes was extensively assessed by MD simulations. The inhibitory activity of the isolated phytoconstituents against tyrosinase was validated by *in vitro* anti-tyrosinase activity experiments. Thus, by integrating theoretical predictions and experimental findings, this work provides intensive perspectives into tyrosinase inhibitory potential *C. spicatum* phenolics. The outcomes of this study are anticipated to significantly contribute to the development of novel melanogenesis inhibitors, potentially applicable in diverse fields.

2. Results and discussion

2.1. Phytochemical investigation

The ethyl acetate soluble fraction of *C. spicatum* ethanolic extract was subjected to successive chromatographic fractionations on different stationary phases. These chromatographic processes led to the isolation of five phenolic compounds isolated for the first time from this species. The chemical structures of isolated phenolics were elucidated based on data obtained from spectroscopic analyses, TLC comparisons with authentic markers, and data comparisons with those previously reported. Thus, EAFCS-isolated phytoconstituents (Figure 1) were identified as isorhamnetin (**1**) [16], cichoric acid (**2**) [17], chlorogenic acid (**3**) [18], gentiopicrin (**4**) [19], and sinapic acid (**5**) [20].

2.2. Molecular docking analysis

Molecular docking calculations of EAFCS-isolated phenolics were executed using AutoDock Vina with the aim of figuring out the binding profile of these phytochemicals with tyrosinase. Table 1 presents the results obtained from molecular docking calculations,

encompassing binding energies, polar interactions, and residues involved in hydrophobic interactions. After numerous iterations considering both binding energies and ligand positioning within the active site of tyrosinase, the energetically favorable docking pose for each compound-enzyme complex was determined. Figures 2-5 illustrate the docking analysis results, depicting the arrangement of various tested phenolics within the active site of the target enzyme. Additionally, these figures highlight the residues involved in polar and hydrophobic interactions with the phytochemicals under investigation. The obtained low binding affinities of isolated phenolics are indicative of the activity of these compounds against the target enzyme.

The outcomes of our docking analysis revealed the successful docking of isolated compounds within the binding site of the target enzyme. Among these compounds, cichoric acid demonstrated the lowest binding affinity (-9.9 kcal/mol), followed by isorhamnetin (-9.3 kcal/mol), gentiopicrin (-9.0 kcal/mol), and chlorogenic acid (-8.1 kcal/mol), while sinapic acid exhibited the highest binding energy (-7.2 kcal/mol). Interestingly, cichoric acid displayed a binding profile identical to that of the standard drug tropolone, as shown in Figure 2. Furthermore, cichoric acid exhibited the highest extent of polar interactions with the target enzyme, forming seven polar bonds, followed by gentiopicrin and chlorogenic acid (six and five polar bonds, respectively). In contrast, isorhamnetin and sinapic displayed a more hydrophobic nature in their binding pathway with the enzyme rather than interacting as polar drugs. This inference is attributed to the existence of only one polar bond and a dense network of hydrophobic interacting residues in the potential binding mechanism of these compounds. Additionally, chlorogenic acid revealed a similar binding profile to the results of the docking run of the standard drug kojic acid (Fig. 5),

6

suggesting its potency as a tyrosinase inhibitor. The results of our molecular docking analysis depicted the variation in residues included in polar interaction with different substrates, indicating a potent inhibitory mechanism for various drugs. Also, the majority of residues involved in the binding profile of these complexes are previously reported as significant key interacting residues in this biologically catalyzed biotransformation [21, 22]. Thus, the results of docking assessments revealed the tyrosinase inhibitory activity of EAFCS-isolated phenolics.

2.3. Molecular dynamics simulations

MD simulation serves as a crucial methodology for comprehensively elucidating the conformational dynamics and molecular behaviors at the atomic scale, as well as unraveling the movement and mechanisms occurring at the molecular level [23, 24]. To explore the compatibility of EAFCS-isolated compounds with the active site of tyrosinase, we executed 30 ns MD simulations to the complex with the lowest binding free energy of each drug using the GROMACS package. A thorough analysis of the 30 ns MD trajectories was conducted, with particular attention directed towards key parameters including root mean square deviations (RMSD), root mean square fluctuations (RMSF), radius of gyration (Rg), solvent accessible surface area (SASA), interaction energies, and hydrogen bonding patterns, for both unbound tyrosinase and the isolated phenolics-tyrosinase complexes.

Analysis of RMSD offers insights into the structural alterations occurring within the molecule throughout MD simulations. The RMSD plot delineates these structural modifications relative to their initial state at 0 ns through the simulation's culmination at 30 ns. As depicted in Figure 6A, during the initial 7ns of the equilibration phase, the RMSD

values of the free enzyme and the complexes of cichoric acid, chlorogenic acid, and gentiopicrin exhibited a fluctuating trend. Subsequently, these RMSD profiles reached equilibrium and sustained within the range of approximately 0.10 to 0.16 nm until the simulation's conclusion. The average RMSD values of unbound tyrosinase and the tyrosinase complexes with cichoric acid, chlorogenic acid, and gentiopicrin are 0.123 nm, 0.124, 0.12, and 0.134 nm, respectively. On the other hand, the complex of the isorhamnetin RMSD profile revealed an upward trend through the first 20 ns of the simulation time. The average RMSD value of the isorhamnetin complex is 0.135 nm, with a high fluctuation pattern within the range of 0.1 to 0.18 nm. The sinapic acid-tyrosinase complex displayed an unexpected RMSD behavior, where the RMSD values reached equilibrium after 7 ns similar to other phenolics, and fluctuated normally within the range of 0.10 to 0.16 nm during the first 25 ns of the simulation span. Then, contrary to other drugs an upward spike was detected after 25 ns. The average RMSD value of the equilibrated portion of the sinapic acid-tyrosinase complex is 0.136 nm. Hence, the results of RMSD analysis of isolated compounds against tyrosinase depicted standard stable trajectories for the tested compounds with a degree of variations in energy-minimized equilibration.

Additionally, the RMSD analysis of ligands (Fig. 6B) revealed a high variation profile for the RMSD values of different phenolics. The highest RMSD was detected for cichoric acid with an average RMSD value of 0.272 nm, followed by the RMSD of chlorogenic acid 0.162 nm. The lowest ligand RMSD pattern was estimated for isorhamnetin with an average of 0.046 nm, meanwhile, the average RMSD values of gentiopicrin and sinapic acid are 0.056 and 0.076 nm, respectively. Although a great variation in RMSD values of different ligands was observed, the RMSD profile of all tested compounds seemed to be

equilibrated and fluctuated normally within the standard range. The higher RMSD values of cichoric acid may suggest its capability to exhibit a specific deviation from the original conformation to fit the enzyme active site. The lower RMSD values of gentiopicrin, sinapic acid, and isorhamnetin suggest that the complexes formed are stable and a small deviation for the ligand's conformation is required for occupying the active site of the enzyme.

Subsequently, we calculated the time-averaged RMSF values for both unbound tyrosinase residues and tyrosinase complexes with isolated phenolics, aiming to evaluate the local protein mobility, as illustrated in Figure 7A. The resulting plot was generated depicting the RMSF values against the residue number throughout a 30 ns trajectory. The RMSF profile generated revealed fluctuations within the catalytic site of tyrosinase, covering a span of approximately 0.03 to 0.44 nm for all systems. Notably, the RMSF value of unbound tyrosinase is lower than those of isolated phenolics-tyrosinase complexes, suggesting that binding of the tested drugs results in stabilization or rustication of the mobility of certain regions within the target enzyme. This stabilization might point out the fact that the isolated phenolics interact with specific residues in the active site, enabling flexibility or fluctuations minimization in the interaction areas. Furthermore, no significant fluctuations were observed at the binding site within the isolated compounds-tyrosinase complexes when compared to the unbound enzyme. Therefore, the data obtained unequivocally corroborate the inference that residues located within the primary binding site experience negligible fluctuations concerning drugs, indicating that the structural integrity of the various drug binding sites remains predominantly stable throughout the 30 ns MD simulations.

The nature of tested phenolics binding within the active site of tyrosinase was investigated by analyzing the hydrogen bonding profile of various complexes throughout the 30 ns MD simulation, as represented in Figure 7B. The results of hydrogen bond monitoring revealed the intensive existence of hydrogen bonding. This outcome is in line with the results of molecular docking analysis. A total of up to seven polar bonds of variable intensities were detected in various studied complexes. The high extent of polar interaction suggests the compatibility of studies phenolics to the active site of tyrosinase.

Temporal fluctuations in the Rg values offer valuable insights into the dynamics of protein folding. These Rg values serve to elucidate the compactness of the enzyme under scrutiny, reflecting its folding and unfolding dynamics over the course of 30 ns molecular dynamics simulations, in accordance with thermodynamic principles [23]. Figure 8A illustrates the computed Rg values for unbound tyrosinase and the studied drugs-tyrosinase complexes over time. Evidently, systems demonstrated stable values around 7 ns, suggesting that tyrosinase and studied complexes reached equilibrium approximately at the 7.5 ns mark of the simulation. Interestingly, the Rg values of unbound tyrosinase are lower than those of complexed counterparts, indicating that the binding of various substrates might cause enzyme compactness or constraining. This could suggest that the binding with isolated phenolics results in reducing the net size or flexibility of tyrosinase, possibly because ligands result in energy minimization in specific regions of inducing conformational alterations that turn tyrosinase into a more compact state. These observations align with previous MD investigations on tyrosinase, suggesting that drug binding diminishes protein compaction and augments its structural compactness [23].

SASA often serves as a metric for quantifying the balance between enzyme-solvent interactions, offering insights into potential conformational changes during the binding process and evaluating protein accessibility [25]. The alterations in SASA for all examined systems throughout the 30 ns MD simulation are shown in Figure 8B. Obviously, the SASA values of free tyrosinase are lower than those of isolated phenolics complexed tyrosinase, suggesting that the binding of phenolics may result in minimizing the overall accessibility of tyrosinase to the surrounding solvent molecules. This could point out the conformational changes induced by different drugs in the active site of the enzyme, enabling a more compact or constrained enzyme structure, and potentially procuring amended protein dynamics or activity. Remarkably, the contrasting trends observed in SASA between free tyrosinase and tyrosinase-ligand complexes mirror the changes observed in Rg values. This consistency affirms the reliability and validity of the results obtained from our MD calculations.

Figure 9 illustrates the Coulomb (Coul) and Lennard-Jones (LJ) interaction energies, derived from GROMACS, between tyrosinase and isolated phenolics throughout the simulation. These energies, extracted from the MD simulation trajectory files, represent short-range (SR) energy interactions. The Coul-SR energy serves as a reliable indicator of the equilibrium state of the drug-enzyme complex throughout the duration of the MD simulation. Also, the values of Coul-SR are considered to be the driving force for the interaction between the target enzyme and the investigated drugs. Table 2 represents the average Gromacs Coul-SR and LJ-SR interaction energies of isolated phenolics-tyrosinase complexes. As shown in Figure 9A, no deviations from the normal fluctuations were detected in the Coul-SR Gromacs energy profile. The interaction of cichoric acid with

11

tyrosinase displayed the lowest Coul-SR interaction energy, averaging -185.849 ± 4.6 kJ/mol (Table 2). This interaction reached equilibrium at approximately 14 ns, after which it fluctuated within the range of approximately -130 to -300 kJ/mol. Interestingly, isorhamnetin displayed a cichoric acid-comparable Coul-SR energy value (-111.429 ± 4.4 kJ/mol) (Table 2). Similar interaction energy patterns were observed for the remaining drugs, albeit with higher interaction energy values. Overall, the Coul-SR interaction energy fluctuations of all tested drugs ranged from 0 to -300 kJ/mol. The more negative the interaction energy values the greater the stability of the complex formed.

On the other hand, the LJ-SR energies were considered reasonable indicators for anticipating binding interactions. Similarly, cichoric acid and isorhamnetin displayed the lowest LJ-SR interaction energy patterns, confirming the potency of these compounds as a tyrosinase inhibitors, as represented in Figure 9B. The average LJ-SR values for cichoric acid and isorhamnetin complexes are -161.612 ± 3.8 kJ/mol and -142.109 ± 2.4, respectively, and it maintains equilibrium after about 14 ns (Table 2). With the exception of chlorogenic acid, all isolated phenolics exhibited typical fluctuation patterns in their LJ-SR energies, fluctuating within the range of approximately -70 to -200 kJ/mol. The highly fluctuating chlorogenic acid LJ-SR profile suggests dynamic and transient interactions between tyrosinase and chlorogenic acid. Additionally, this elevated fluctuation suggests that the formed complex is continuously subjected to conformational adjustment and orientation, possibly reflecting the dynamic favorable binding and drug unbinding from the active site along the course of the simulation.

Thus, the lower Coul-SR than their LJ-SR counterparts suggests a weaker electrostatic interaction than the van der Waals interactions among various complex constituting atoms.

This outcome leads to the conclusion that some of the formed complexes are stabilized by hydrophobic interactions such as dispersion forces rather than by electrostatic interactions. In addition, the normal fluctuation and more negative Coul-SR and LJ-SR values suggest relatively balanced and stable isolated phenolics-tyrosinase interactions. Consequently, the complexes are kinetically and energetically favored, excluding neither weak nor strong dominating interactions. Also, minor conformational adjustments and fluctuation around the thermodynamically favorable state were predicted for various complexes, indicating a stable and dynamically balanced binding mode.

2.4. *In vitro* tyrosinase inhibition

The activities of the isolated phenolics as anti-tyrosinase inhibitors were evaluated using an *in vitro* tyrosinase inhibition assay (Figure 10). Among the tested compounds, cichoric acid exhibited the lowest IC_{50} value, indicating its potent inhibitory effect against tyrosinase. Following cichoric acid, isorhamnetin displayed a moderately low IC_{50} value, suggesting its significant inhibitory activity against the enzyme. Gentiopicrin showed a slightly higher IC_{50} value followed by chlorogenic acid, while sinapic acid exhibited the highest IC_{50} value among the tested compounds. These experimental findings align with the results obtained from docking and MD simulations. Specifically, cichoric acid and isorhamnetin demonstrated the lowest docking binding affinity values and Gromacs interaction energy values, further corroborating their potency as tyrosinase inhibitors. The agreement between the results of the *in vitro* tyrosinase inhibition assay and our computational methods conducted *in silico* provides strong validation for our computational approaches. Overall, our results collectively indicate that cichoric acid and isorhamnetin hold promise as effective agents for inhibiting tyrosinase activity, offering

potential therapeutic applications in conditions associated with aberrant melanin production.

Due to their notable activity among tested compounds, as indicated by its lowest IC_{50} value and high inhibition rate, cichoric acid was singled out for further scrutiny regarding its enzyme kinetics. It displayed a pronounced inhibitory effect against tyrosinase *in vitro*, effectively diminishing enzyme activity even at relatively low concentrations as depicted in Figure 11. The concentration-dependent response signifies a correlation between the inhibitor concentration and the degree of enzymatic inhibition, indicating a concentration-dependent relationship. Lineweaver–Burk analysis revealed that cichoric acid effectively inhibited tyrosinase-mediated L-DOPA hydrolysis through a mixed inhibition mechanism (Fig. 11B), and the calculated inhibition constant (K_i) value was 1.64 μM. These findings advocate for further exploration of the potential efficacy of cichoric acid as a tyrosinase inhibitor for therapeutic purposes.**3. Conclusion**

The results of chromatographic fractionation of EAFCS afforded five known phenolics reported for the first time from this species. The activities of the isolated phytochemicals as tyrosinase inhibitors were assessed by a combination of both *in vitro* and *in silico* approaches. Based on the results of molecular docking analysis, the isolated compounds were shown to dock into the main binding site of tyrosinase. Cichoric acid displayed the lowest binding affinity and the highest number of polar interactions with residues in the active site of tyrosinase, suggesting its superior activity against tyrosinase. Compounds **1** and **5** displayed a more hydrophobic nature in their binding pathways, with compound **4** showing intermediate characteristics. These findings suggest a potent inhibitory mechanism for the various drugs, with residues involved in the binding profile of these

14

complexes aligning with previously reported key interacting residues in tyrosinase catalysis. In addition, we utilized MD simulations to investigate the compatibility of phenolics isolated from *C. spicatum* with the active site of tyrosinase. Through 30 ns MD simulations, we analyzed various parameters including RMSD, RMSF, Rg, SASA, interaction energies, and hydrogen bonding profiles. Our analysis revealed stable trajectories for the tested compounds, with a degree of energy-minimized equilibration observed for cichoric acid. Additionally, the hydrogen bonding profiles suggested strong interactions between the phenolics and the active site of tyrosinase. The calculated time-averaged RMSF values indicated that the binding of the phenolics stabilized the mobility of certain regions within the enzyme. Furthermore, the analysis of Rg and SASA values showed that the binding of phenolics reduced the flexibility and accessibility of tyrosinase, supporting the stability of the drug-enzyme complexes. Finally, the examination of Coul-SR and LJ-SR energies revealed a balanced and stable interaction between the phenolics and tyrosinase, predominantly stabilized by hydrophobic interactions, with the minimum interaction energies in both cases for cichoric acid. The results of *in vitro* tyrosinase inhibition assay displayed the lowest IC_{50} value for cichoric acid, confirming its potency as a tyrosinase inhibitor. Moreover, cichoric acid demonstrated a mixed inhibition mode against tyrosinase-mediated L-DOPA hydrolysis. The congruence between the outcomes of the *in vitro* tyrosinase inhibition assay and our *in-silico* methodologies serves as a robust validation of our computational approaches. Overall, these findings provide valuable insights into the mechanism of action of phenolics from *C. spicatum* as tyrosinase inhibitors, laying the groundwork for further development of novel melanogenesis inhibitors with potential therapeutic applications.

4. Materials and Methods

4.1. General

Nuclear magnetic resonance (NMR) spectra of the isolated compounds were acquired using a Bruker AM-500 spectrometer operating at 500 MHz for ^{1}H NMR and 100 MHz for ^{13}C NMR. The optical rotation was determined using a Rudolph Autopol III polarimeter. UV spectra were recorded using a Shimadzu UV–Vis 160i spectrophotometer. High-resolution electron ionization mass spectrometry (HREIMS) and electron ionization mass spectrometry (EIMS) analyses were conducted using a Finnigan MAT TSQ 700 mass spectrometer. Fourier-transform infrared (FTIR) spectra were obtained using a Shimadzu FTIR-8400 instrument with potassium bromide (KBr) pellets.

4.2. Plant collection, extraction, and isolation of phytochemicals

The aerial parts of *C. spicatum* were collected from the western desert area close to Beni-Suef governorate in May 2022. Identification of the plant was performed by taxonomists from the Botany Department at Beni-Suef University. The collected plant was air-dried and grounded, and 4 kg was extracted with 70% ethanol by cold maceration. Then, the extraction solvent was removed under reduced pressure to afford a sticky mass of the crude extract weighing 267 g. A solvent-solvent partition process was applied to the crude extract employing ethyl acetate, *n*-butanol, and *n*-hexane as partitioning solvents. Based on the TLC profile, ethyl acetate fraction (EAFCS) was selected for further chromatographic investigation for the phytochemicals. An amount of 25 g of dried ethyl acetate fraction, after solvent removal *in vacuo*, was subjected to fractionation over a silica gel column (100 × 3.5 cm, 0.75 kg) eluted with dichloromethane: methanol solvent system (10:0 to 0:10).

UV light was utilized to facilitate the fractionation process by monitoring the migration of bands along the column. A total of 12 fractions were collected and subsequently pooled into three fractions (designated as E1-E3) based on their TLC behavior. Fraction E1 was further chromatographed over a silica gel column (50 × 2 cm) eluted with a hexane/ethyl acetate solvent system of increasing polarity as an eluent to afford 9 subfractions (S1-S9). Subfractions S3-S7 were combined because of their similar TLC profile and further chromatographed over Sephadex LH-20 column using methanol as an eluent to give the purified compounds **3** (17 mg) and **5** (21 mg). Fraction E2 was placed on the top of a polyamide 6s column (30 × 1.5 cm) using methanol as an eluent. The effluent from the column was consolidated into 7 subfractions (T1-T7) based on the TLC profile. The purified compounds **2** (16 mg) and **4** (19 mg) were obtained from further fractionation of the combined subfraction T2-T5 on the Sephadex LH-20 column using methanol as an eluent. Chromatographic fractionation of Fraction 3 on silica gel column (50 × 2 cm) eluted with ethyl acetate/dichloromethane system of increasing polarity afforded main four subfractions (Z1-Z4). The major subfraction Z2 was subjected to purification over the Sephadex LH-20 column using methanol to produce compound **1** (23 mg).

4.3. Molecular docking

The binding energies of EAFCS-isolated phenolics with the crystal structure of tyrosinase were calculated using AutoDock Vina and Autodock Tools (ADT) v1.5.6 software package [26]. The initial structures of EAFCS-derived phytochemicals were geometrically optimized at the B3LYP level [27-29] with the 6-311G (d, p) basis set [30] using the Gaussian 16 software package [31]. The three-dimensional crystalline configuration of human tyrosinase was procured from the Protein Data Bank under the identification code

5M8Q. The molecular docking procedure and steps were implemented as we previously reported [25, 32, 33].

4.4. Molecular dynamics simulations

The MD simulations commenced with the utilization of the PDB file representing the EAFCS-isolated phytochemicals-tyrosinase complexes featuring the lowest binding energy, which was identified through molecular docking analysis. These simulations, spanning 30 ns, encompassed both tyrosinase in an aqueous environment and the isolated phenolics-tyrosinase complexes, and were conducted using the GROMACS 2022.4 software package [34-36]. The all-atom MD runs for unbound tyrosinase and the isolated compound-tyrosinase complexes employed the structure-balanced CHARMM36m force field [37]. Topology and geometric parameters for studied phytoconstituents were generated utilizing CGenFF (https://cgenff.umaryland.edu/). Enclosed within a dodecahedron box under periodic boundary conditions, both the complexes and enzyme occupied a new box volume of 515.79 nm^3. Solvation was achieved using the CHARMM-modified TIP3P water model [38], and electro-neutrality was maintained by introducing 12 sodium counter-ions. To mitigate unfavorable thermodynamic interactions, the steepest descent energy minimization technique was applied for 10 picoseconds (ps) [34]. Following this, both systems underwent two stages of equilibration at 300 K for 100 ps each, utilizing NVT and NPT ensembles [39]. Subsequently, MD simulations were conducted throughout 30 ns at a temperature of 300 K and pressure of 1 bar, following a protocol established in previous studies [23, 40, 41].

4.5. *In vitro* tyrosinase inhibition assay

The inhibitory activity of the isolated compounds against tyrosinase was determined using the modified dopachrome method as described by Masuda et al [42] and Alam et al [43]. The sample (compounds **1**-**5** and kojic acid (Sigma, USA) dissolved in DMSO) was mixed with the same volume of mushroom tyrosinase (31 U/ml; Sigma, USA) and L-DOPA (2.5 mM; Sigma, USA) and double volume of 50 mM phosphate buffer (pH 6.8). The mixture was incubated at 37°C for 10 min followed by measurement of the absorbance at 475 nm. The experiment was conducted in triplicate. The inhibition kinetics of cichoric acid on tyrosinase were analyzed using Lineweaver–Burk plots. K_i value was derived from secondary plots depicting the apparent K_m/V_{max} or $1/V_{max}$ versus the concentrations of the inhibitor. The value was calculated by the nonlinear regression assessments of GraphPad Prism 9.0 software (San Diego, CA, USA).

Author Contributions

Conceptualization, A.M.M., A-M.L., and E.M.K.; methodology, R.S.A., A.M.M., A-M.L., A.A.E., I.E., A.F.A., and E.M.K.; software, A-M.L. and E.M.K; validation, A.M.M., A-M.L., and E.M.K.; formal analysis, A.M.M., and E.M.K.; investigation, R.S.A., A.M.M., A-M.L., A.A.E., and E.M.K.; resources, R.S.A., A.F.A., and A-M.L.; data curation, R.S.A., E.M.K., and A.M.M.; writing—original draft preparation, E.M.K., and A.M.M.; writing—review and editing, A.M.M., and A-M.L.; visualization, E.M.K., and A.M.M.; supervision, A.M.M., and A-M.L.; project administration, R.S.A. and A.M.M.; funding acquisition, R.S.A. All authors have read and agreed to the published version of the manuscript.

Acknowledgment

Declaration of Competing Interest

All authors declare no conflicts of interest in relation to the manuscript.

Availability of data and materials

The manuscript contains all data supporting the reported results.

References
[1] C.S. Nunes, K. Vogel, Chapter 20 - Tyrosinases—physiology, pathophysiology, and applications, in: C.S. Nunes, V. Kumar (Eds.), Enzymes in Human and Animal Nutrition, Academic Press2018, pp. 403-412.
[2] X. Li, J. Guo, J. Lian, F. Gao, A.J. Khan, T. Wang, F. Zhang, Molecular Simulation Study on the Interaction between Tyrosinase and Flavonoids from Sea Buckthorn, ACS Omega 6(33) (2021) 21579-21585.
[3] R. Logesh, S.R. Prasad, S. Chipurupalli, N. Robinson, S.K. Mohankumar, Natural tyrosinase enzyme inhibitors: A path from melanin to melanoma and its reported pharmacological activities, Biochimica et Biophysica Acta (BBA) - Reviews on Cancer 1878(6) (2023) 188968.
[4] P. Rathee, S. Kumar, D. Kumar, B. Kumari, S.S. Yadav, Skin hyperpigmentation and its treatment with herbs: an alternative method, Future Journal of Pharmaceutical Sciences 7(1) (2021) 132.
[5] B. Roulier, B. Pérès, R. Haudecoeur, Advances in the Design of Genuine Human Tyrosinase Inhibitors for Targeting Melanogenesis and Related Pigmentations, Journal of Medicinal Chemistry 63(22) (2020) 13428-13443.
[6] G. Tovilovic-Kovacevic, N. Zogovic, D. Krstic-Milosevic, Chapter 19 - Secondary metabolites from endangered Gentiana, Gentianella, Centaurium, and Swertia species (Gentianaceae): promising natural biotherapeutics, in: M. Ozturk, D. Egamberdieva, M. Pešić (Eds.), Biodiversity and Biomedicine, Academic Press2020, pp. 335-384.

[7] J. Božunović, M. Ivanov, J. Petrović, U. Gašić, Đ. Nakarada, M. Milutinović, N. Aničić, Z. Giba, D. Mišić, D. Stojković, Solvent System-Guided Extraction of Centaurium spicatum (L.) Fritch Provides Optimized Conditions for the Biological and Chemical Characteristics of the Herbal Extracts, Pharmaceuticals 16(2) (2023) 245.

[8] Z. Peng, J. He, Y. Cheng, J. Xu, W. Zhang, Biologically active secoiridoids: A comprehensive update, Medicinal Research Reviews 43(4) (2023) 1201-1252.

[9] G. Zengin, M. El-Raey, W. El-Kashak, G.E.-S. Batiha, D. Althumairy, S. Alamer, N.M. Mostafa, O.A. Eldahshan, Sweroside: An iridoid glycoside of potential neuroprotective, antidiabetic, and antioxidant activities supported by molecular docking, Amino Acids 55(12) (2023) 1765-1774.

[10] B. Šiler, D. Mišić, Chapter 11 - Biologically Active Compounds from the Genus Centaurium s.l. (Gentianaceae): Current Knowledge and Future Prospects in Medicine, in: R. Atta ur (Ed.), Studies in Natural Products Chemistry, Elsevier2016, pp. 363-397.

[11] R.S. Alruhaimi, G. Mostafa-Hedeab, M.S. Abduh, A. Bin-Ammar, E.H.M. Hassanein, E.M. Kamel, A.M. Mahmoud, A flavonoid-rich fraction of Euphorbia peplus attenuates hyperglycemia, insulin resistance, and oxidative stress in a type 2 diabetes rat model, Frontiers in Pharmacology 14 (2023).

[12] R.S. Alruhaimi, E.H.M. Hassanein, M.K. Abd El-Aziz, M. Siddiq Abduh, A. Bin-Ammar, E.M. Kamel, A.M. Mahmoud, The melatonin receptor agonist agomelatine protects against acute pancreatitis induced by cadmium by attenuating inflammation and oxidative stress and modulating Nrf2/HO-1 pathway, International Immunopharmacology 124 (2023) 110833.

[13] D.H. Sami, A.S. Soliman, A.A. Khowailed, R.S. Alruhaimi, E.H.M. Hassanein, E.M. Kamel, A.M. Mahmoud, The protective effect of 7-hydroxycoumarin against cisplatin-induced liver injury is mediated via attenuation of oxidative stress and inflammation and upregulation of Nrf2/HO-1 pathway, Environmental Science and Pollution Research 30(33) (2023) 80181-80191.

[14] R. Shukla, T. Tripathi, Molecular Dynamics Simulation of Protein and Protein–Ligand Complexes, in: D.B. Singh (Ed.), Computer-Aided Drug Design, Springer Singapore, Singapore, 2020, pp. 133-161.

[15] E. Gayathiri, P. Prakash, P. Kumaravel, J. Jayaprakash, M.G. Ragunathan, S. Sankar, S. Pandiaraj, N. Thirumalaivasan, M. Thiruvengadam, R. Govindasamy, Computational approaches for modeling and structural design of biological systems: A comprehensive review, Progress in Biophysics and Molecular Biology 185 (2023) 17-32.

[16] X. Cao, Y. Wei, Y. Ito, Preparative Isolation of Isorhamnetin from Stigma Maydis using High Speed Countercurrent Chromatography, Journal of Liquid Chromatography & Related Technologies 32(2) (2008) 273-280.

[17] Z. Luo, G. Gao, Z. Ma, Q. Liu, X. Gao, X. Tang, Z. Gao, C. Li, T. Sun, Cichoric acid from witloof inhibit misfolding aggregation and fibrillation of hIAPP, International Journal of Biological Macromolecules 148 (2020) 1272-1279.

[18] J.X. Cheng, Y.Q. Li, J. Cai, C.F. Zhang, T. Akihisa, W. Li, T. Kikuchi, W.Y. Liu, F. Feng, J. Zhang, Phenolic compounds from Ficus hispida L.f. as tyrosinase and melanin inhibitors: Biological evaluation, molecular docking, and molecular dynamics, Journal of Molecular Structure 1244 (2021) 130951.

[19] L. Zhang, E.S. Ulriksen, H. Hoel, L. Sandvik, K.E. Malterud, K.T. Inngjerdingen, M. Inngjerdingen, H. Wangensteen, Phytochemical characterization and anti-inflammatory activity of a water extract of Gentiana purpurea roots, Journal of Ethnopharmacology 301 (2023) 115818.

[20] J. Li, Z. Guo, Identification and quantification of phenolic compounds in rapeseed originated lecithin and antioxidant activity evaluation, LWT 73 (2016) 397-405.

[21] Y. Jung Park, H. Jin Jung, H. Jin Kim, H. Soo Park, J. Lee, D. Yoon, M. Kyung Kang, G. Young Kim, S. Ullah, D. Kang, Y. Park, P. Chun, H. Young Chung, H. Ryong Moon, Thiazol-4(5H)-one analogs as potent tyrosinase inhibitors: Synthesis, tyrosinase inhibition, antimelanogenic effect, antioxidant activity, and in silico docking simulation, Bioorganic & Medicinal Chemistry 98 (2024) 117578.

[22] A. Kumari, R. kumar, G. Sulabh, P. Singh, J. Kumar, V.K. Singh, K.K. Ojha, In silico ADMET, molecular docking and molecular simulation-based study of glabridin's natural and semisynthetic derivatives as potential tyrosinase inhibitors, Advances in Traditional Medicine 23(3) (2023) 733-751.

[23] E.M. Kamel, A.M. Lamsabhi, The quasi-irreversible inactivation of cytochrome P450 enzymes by paroxetine: a computational approach, Organic & Biomolecular Chemistry 18(17) (2020) 3334-3345.

[24] E.M. Kamel, A.M. Lamsabhi, Water biocatalytic effect attenuates cytochrome P450-mediated carcinogenicity of diethylnitrosamine: A computational insight, Organic & Biomolecular Chemistry 19(41) (2021) 9031-9042.

[25] E.M. Kamel, A. Bin-Ammar, A.A. El-Bassuony, M.M. Alanazi, A. Altharawi, A.F. Ahmeda, A.S. Alanazi, A.M. Lamsabhi, A.M. Mahmoud, Molecular modeling and DFT studies on the antioxidant activity of Centaurea scoparia flavonoids and molecular dynamics simulation of their interaction with β-lactoglobulin, RSC Advances 13(18) (2023) 12361-12374.

[26] O. Trott, A.J. Olson, AutoDock Vina: Improving the speed and accuracy of docking with a new scoring function, efficient optimization, and multithreading, Journal of Computational Chemistry 31(2) (2010) 455-461.

[27] A.D. Becke, Density-functional thermochemistry. III. The role of exact exchange, The Journal of Chemical Physics 98(7) (1993) 5648-5652.

[28] C. Lee, W. Yang, R.G. Parr, Development of the Colle-Salvetti correlation-energy formula into a functional of the electron density, Physical review B 37(2) (1988) 785.

[29] A.D. Becke, Density-functional exchange-energy approximation with correct asymptotic behavior, Physical review A 38(6) (1988) 3098.

[30] W.J. Hehre, L. Radom, P.v.R. Schleyer, J.A. Pople, Ab initio molecular orbital theory, Wiley New York et al.1986.

[31] M.J. Frisch, G.W. Trucks, H.B. Schlegel, G.E. Scuseria, M.A. Robb, J.R. Cheeseman, G. Scalmani, V. Barone, G.A. Petersson, H. Nakatsuji, X. Li, M. Caricato, A.V. Marenich, J. Bloino, B.G. Janesko, R. Gomperts, B. Mennucci, H.P. Hratchian, J.V. Ortiz, A.F. Izmaylov, J.L. Sonnenberg, Williams, F. Ding, F. Lipparini, F. Egidi, J. Goings, B. Peng, A. Petrone, T. Henderson, D. Ranasinghe, V.G. Zakrzewski, J. Gao, N. Rega, G. Zheng, W. Liang, M. Hada, M. Ehara, K. Toyota, R. Fukuda, J. Hasegawa, M. Ishida, T. Nakajima, Y. Honda, O. Kitao, H. Nakai, T. Vreven, K. Throssell, J.A. Montgomery Jr., J.E. Peralta, F. Ogliaro, M.J. Bearpark, J.J. Heyd, E.N. Brothers, K.N. Kudin, V.N. Staroverov, T.A. Keith, R. Kobayashi, J. Normand, K. Raghavachari, A.P. Rendell, J.C. Burant, S.S. Iyengar, J.

Tomasi, M. Cossi, J.M. Millam, M. Klene, C. Adamo, R. Cammi, J.W. Ochterski, R.L. Martin, K. Morokuma, O. Farkas, J.B. Foresman, D.J. Fox, Gaussian 16 Rev. C.01, Wallingford, CT, 2016.

[32] E.M. Kamel, N.A. Ahmed, A.A. El-Bassuony, O.E. Hussein, B. Alrashdi, S.A. Ahmed, A.M. Lamsabhi, H.H. Arab, A.M. Mahmoud, Xanthine oxidase inhibitory activity of Euphorbia peplus L. phenolics, Combinatorial Chemistry & High Throughput Screening 25(8) (2022) 1336-1344.

[33] E.M. Kamel, A.M. Tawfeek, A.A. El-Bassuony, A.M. Lamsabhi, Mechanistic aspects of reactive metabolite formation in clomethiazole catalyzed biotransformation by cytochrome P450 enzymes, Organic & Biomolecular Chemistry (2023).

[34] P. Bauer, B. Hess, E. Lindahl, GROMACS 2022.4 Manual, November 16 (2022) 2022.

[35] M.J. Abraham, T. Murtola, R. Schulz, S. Páll, J.C. Smith, B. Hess, E. Lindahl, GROMACS: High performance molecular simulations through multi-level parallelism from laptops to supercomputers, SoftwareX 1-2 (2015) 19-25.

[36] B. Hess, C. Kutzner, D. van der Spoel, E. Lindahl, GROMACS 4: Algorithms for Highly Efficient, Load-Balanced, and Scalable Molecular Simulation, Journal of Chemical Theory and Computation 4(3) (2008) 435-447.

[37] J. Huang, S. Rauscher, G. Nawrocki, T. Ran, M. Feig, B.L. de Groot, H. Grubmüller, A.D. MacKerell, Jr., CHARMM36m: an improved force field for folded and intrinsically disordered proteins, Nat Methods 14(1) (2017) 71-73.

[38] A.D. MacKerell, Jr., D. Bashford, M. Bellott, R.L. Dunbrack, Jr., J.D. Evanseck, M.J. Field, S. Fischer, J. Gao, H. Guo, S. Ha, D. Joseph-McCarthy, L. Kuchnir, K. Kuczera, F.T.K. Lau, C. Mattos, S. Michnick, T. Ngo, D.T. Nguyen, B. Prodhom, W.E. Reiher, B. Roux, M. Schlenkrich, J.C. Smith, R. Stote, J. Straub, M. Watanabe, J. Wiórkiewicz-Kuczera, D. Yin, M. Karplus, All-Atom Empirical Potential for Molecular Modeling and Dynamics Studies of Proteins, The Journal of Physical Chemistry B 102(18) (1998) 3586-3616.

[39] M. Parrinello, A. Rahman, Polymorphic transitions in single crystals: A new molecular dynamics method, Journal of Applied physics 52(12) (1981) 7182-7190.

[40] J.A. Lemkul, From Proteins to Perturbed Hamiltonians: A Suite of Tutorials for the GROMACS-2018 Molecular Simulation Package [Article v1.0], Living Journal of Computational Molecular Science 1(1) (2018) 5068.

[41] E.M. Kamel, A.M. Tawfeek, A.A. El-Bassuony, A.M. Lamsabhi, Mechanistic insights into chloramphenicol-mediated inactivation of cytochrome P450 enzymes and their active site mutants, New Journal of Chemistry 47(35) (2023) 16429-16443.

[42] T. Masuda, D. Yamashita, Y. Takeda, S. Yonemori, Screening for Tyrosinase Inhibitors among Extracts of Seashore Plants and Identification of Potent Inhibitors from Garcinia subelliptica, Bioscience, Biotechnology, and Biochemistry 69(1) (2005) 197-201.

[43] N. Alam, K.N. Yoon, K.R. Lee, P.G. Shin, J.C. Cheong, Y.B. Yoo, J.M. Shim, M.W. Lee, U.Y. Lee, T.S. Lee, Antioxidant Activities and Tyrosinase Inhibitory Effects of Different Extracts from Pleurotus ostreatus Fruiting Bodies, Mycobiology 38(4) (2010) 295-301.

Tables:

Table 1. Results of molecular docking analysis of EAFCS-isolated phenolics against tyrosinase.

Compounds	Binding affinity (kcal/mol)	Polar interacting residues	Hydrophobic interacting residues
1	-9.3	Trp117	Ser106, Cys113, Arg114, Pro115, Gly116, Arg118, Val126, Tyr226, Leu229, Lys233, Arg230, and Pro445
2	-9.9	Cys101, Gly103, Ser106, Gly107, Gly116, Tyr226, Arg230, and Gln236	Phe105, Thr112, Arg114, Pro115, Ile128, Leu229, Glu232, Lys233, Pro445, and Met452
3	-8.1	Val196, Val211, Asp212, Gly389, and Ser394	His192, Gly209, His215, Glu216, His377, His381, Leu382, Gln390, and Val391
4	-9.0	Arg114, Gly116, Trp117, Arg118, Lys233, and Pro242	Thr112, Pro115, Val126, Ile128, Gln236, Glu137, and Glu241
5	-7.2	Tyr226	Pro115, Gly116, Trp117, Val126, Leu229, Arg230, Lys233, Glu232, Leu460, and Tyr462
Kojic acid	-5.8	Asn378, and Ser394	Phe362, His215, Val391, His192, Gln390, His381, Gly388, and Gly389
Tropolone	-6.1	Ser106, Cys113, and Arg230	Pro115, Tyr226, Leu229, and Lys233

Table 2. Gromacs average Coul-SR and LJ-SR interaction energies of isolated phenolics-tyrosinase complexes.

	Average Coul-SR interaction energy (kJ/mol)	Average LJ-SR interaction energy (kJ/mol)
Isorhamnetin-tyrosinase	-111.429 ± 4.4	-142.109 ± 2.4
Cichoric acid-tyrosinase	-185.849 ± 4.6	-161.612 ± 3.8
Chlorogenic acid-tyrosinase	-50.836 ± 5.7	-109.587± 6.1
Gentiopicrin-tyrosinase	-78.455 ± 7.2	-107.335 ± 7.3
Sinapic acid-tyrosinase	-47.782 ± 5.1	-108.275 ± 1.4

Figures:
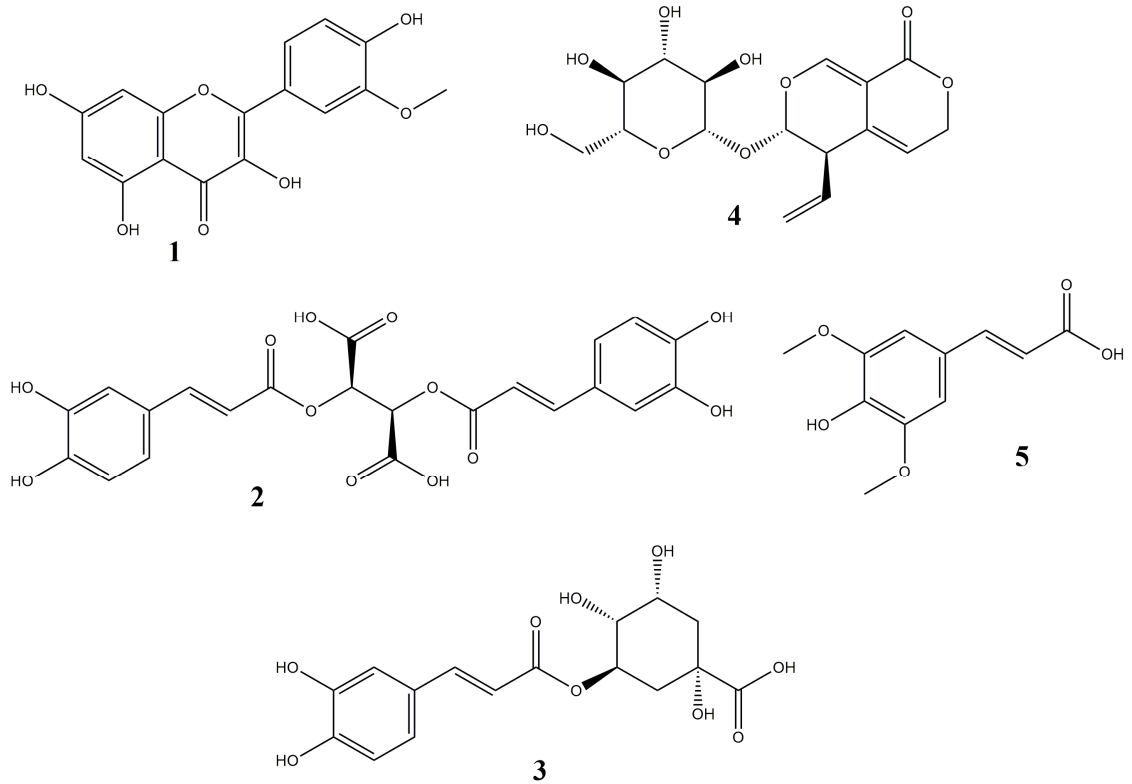
Figure 1. Structures of EAFCS-isolated compounds.
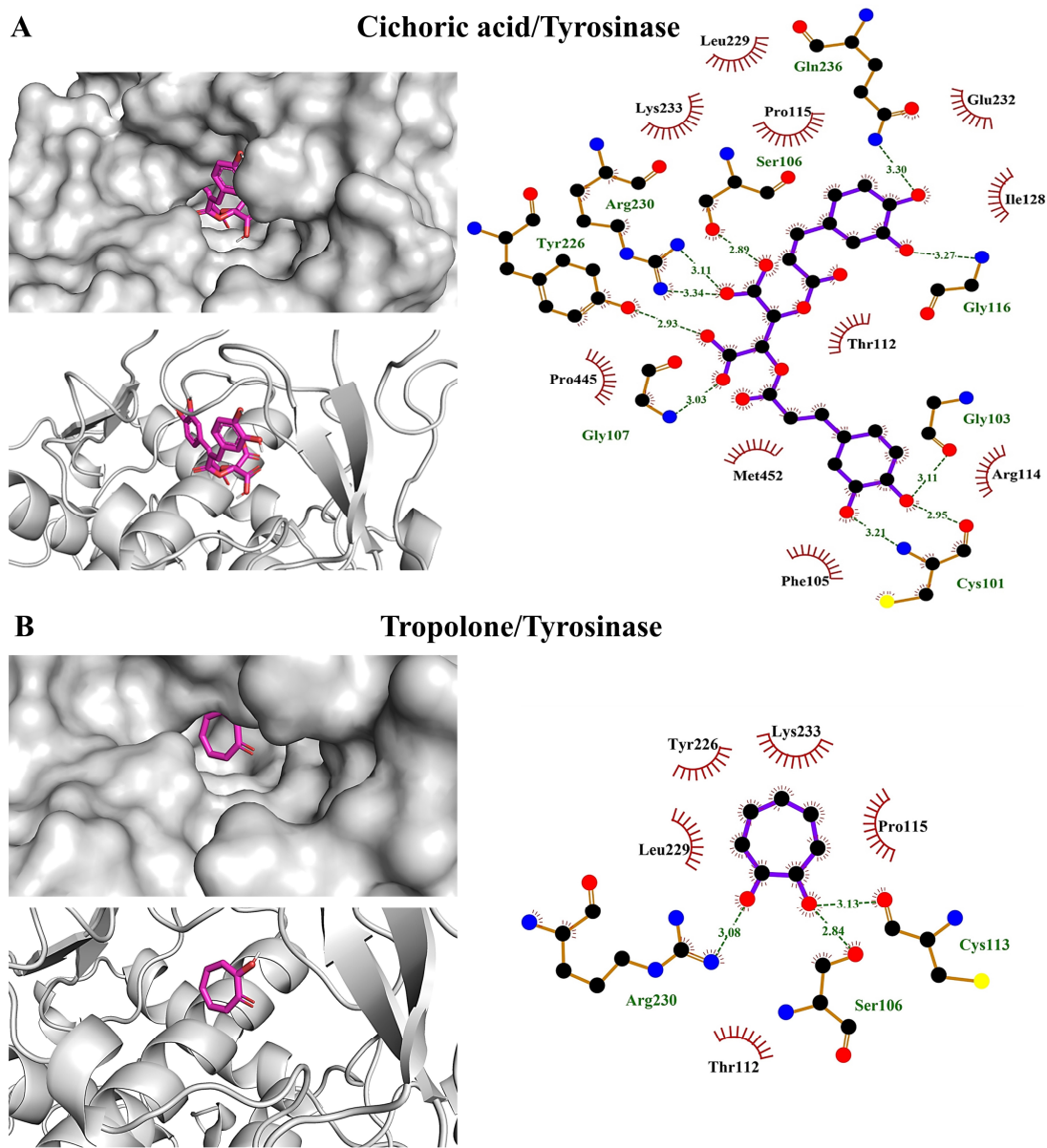
Figure 2. Binding site interactions of cichoric acid (A) and tropolone (B) with tyrosinase.
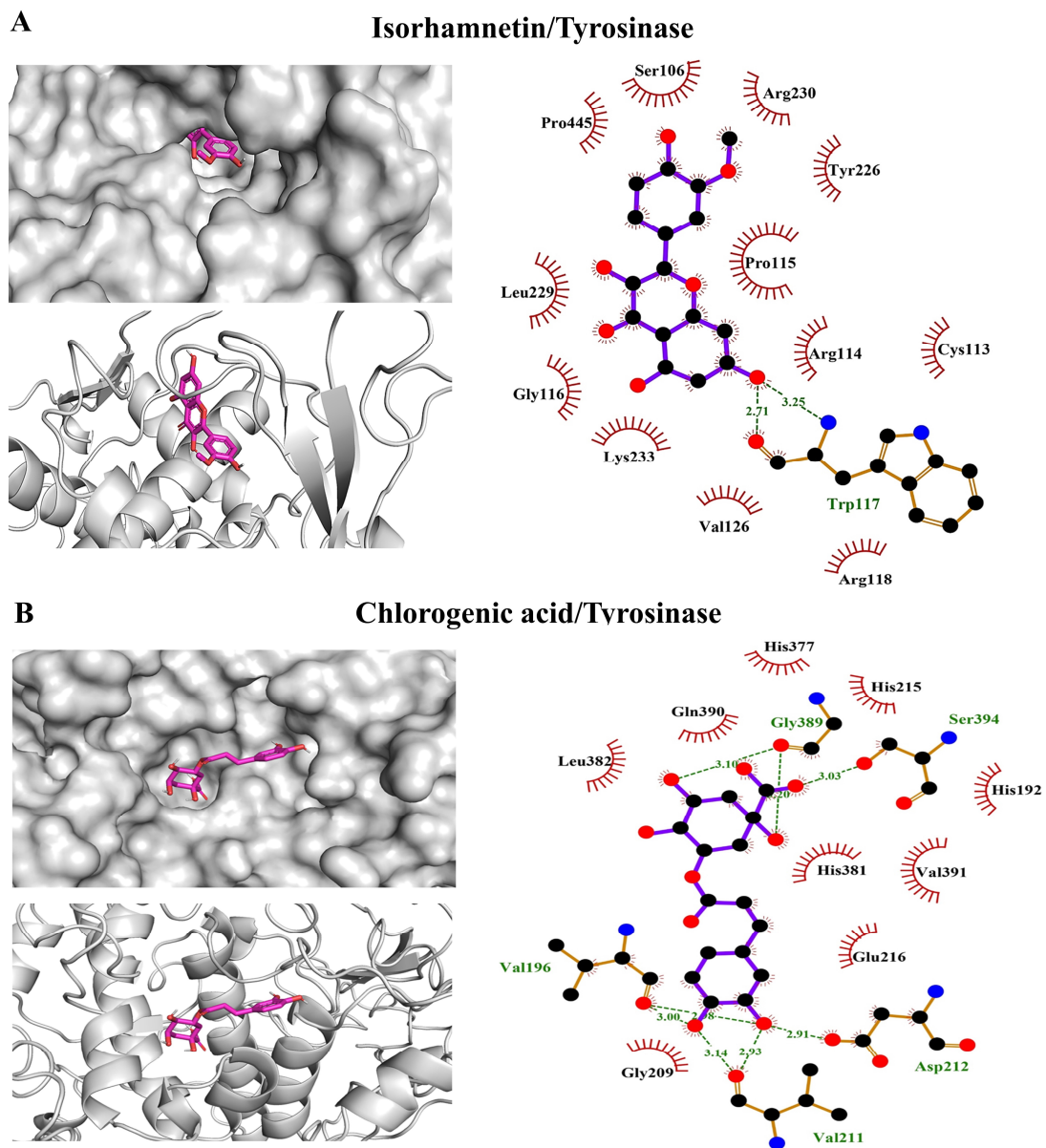
Figure 3. Binding site interactions of isorhamnetin (A) and chlorogenic acid (B) with tyrosinase.
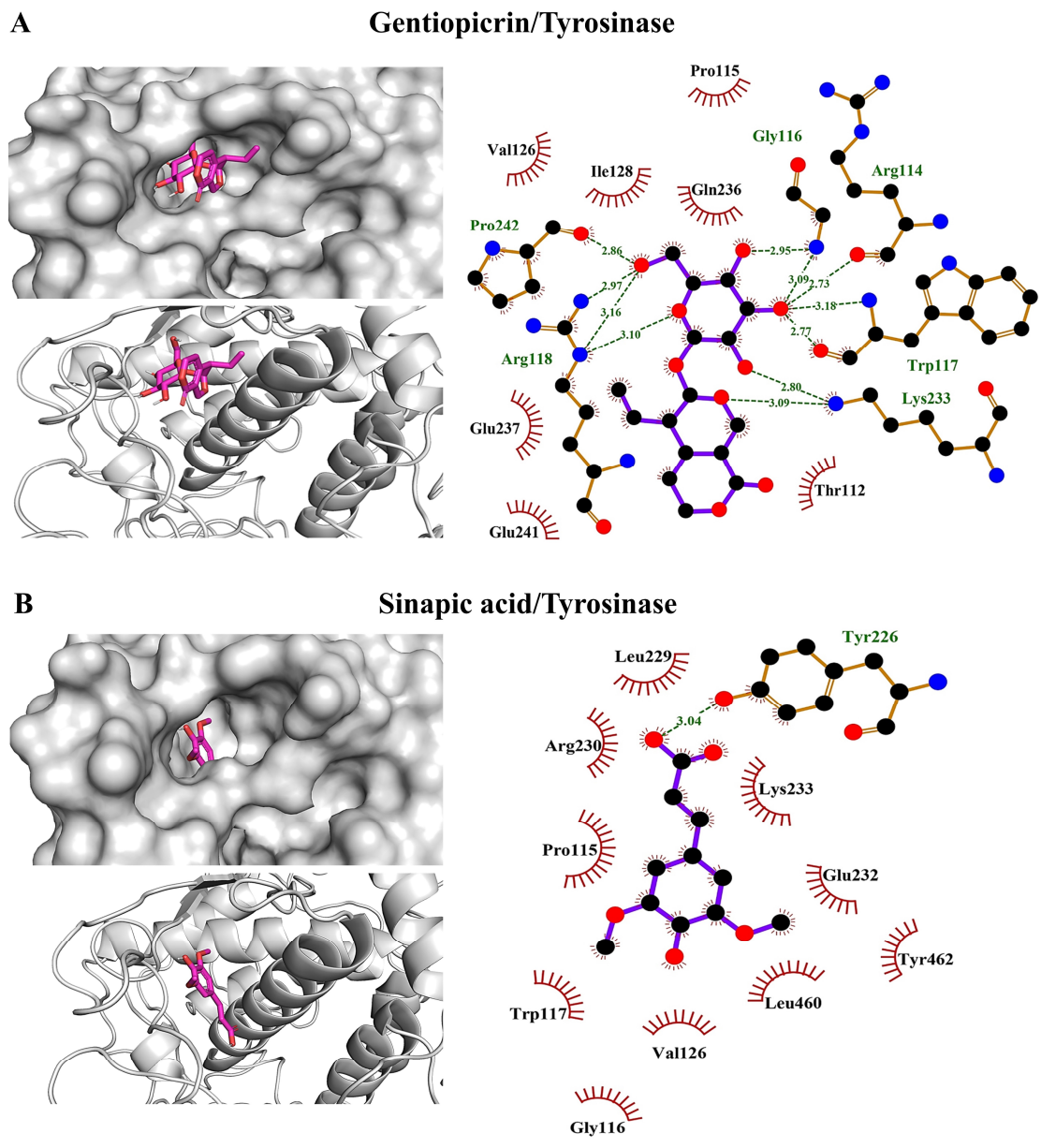
Figure 4. Binding site interactions of gentiopicrin (A) and sinapic acid (B) with tyrosinase.
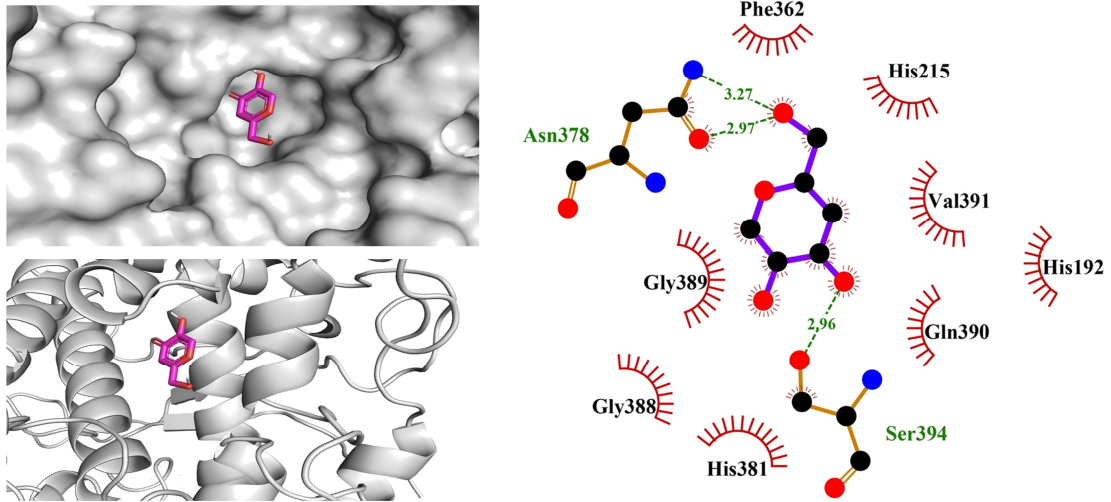
Kojic acid/Tyrosinase

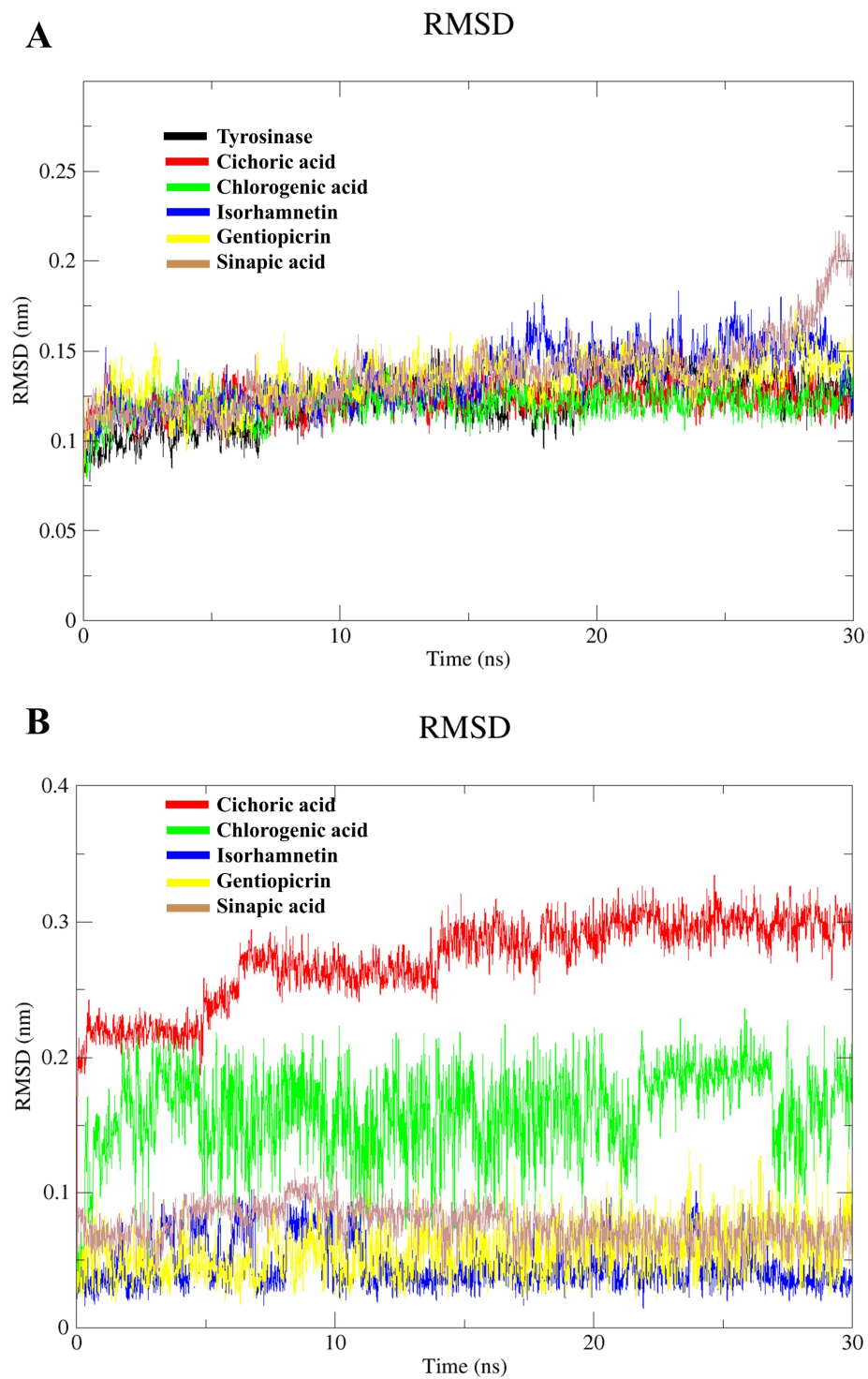Figure 5. Binding site interactions of kojic acid with tyrosinase.

Figure 6. MD simulation (30 ns) analysis of tyrosinase and various EAFCS-isolated phenolics-tyrosinase complexes; (A) Backbone RMSD of the unbound tyrosinase and isolated compounds-tyrosinase complexes and (B) RMSD of isolated drugs.

A RMS fluctuation
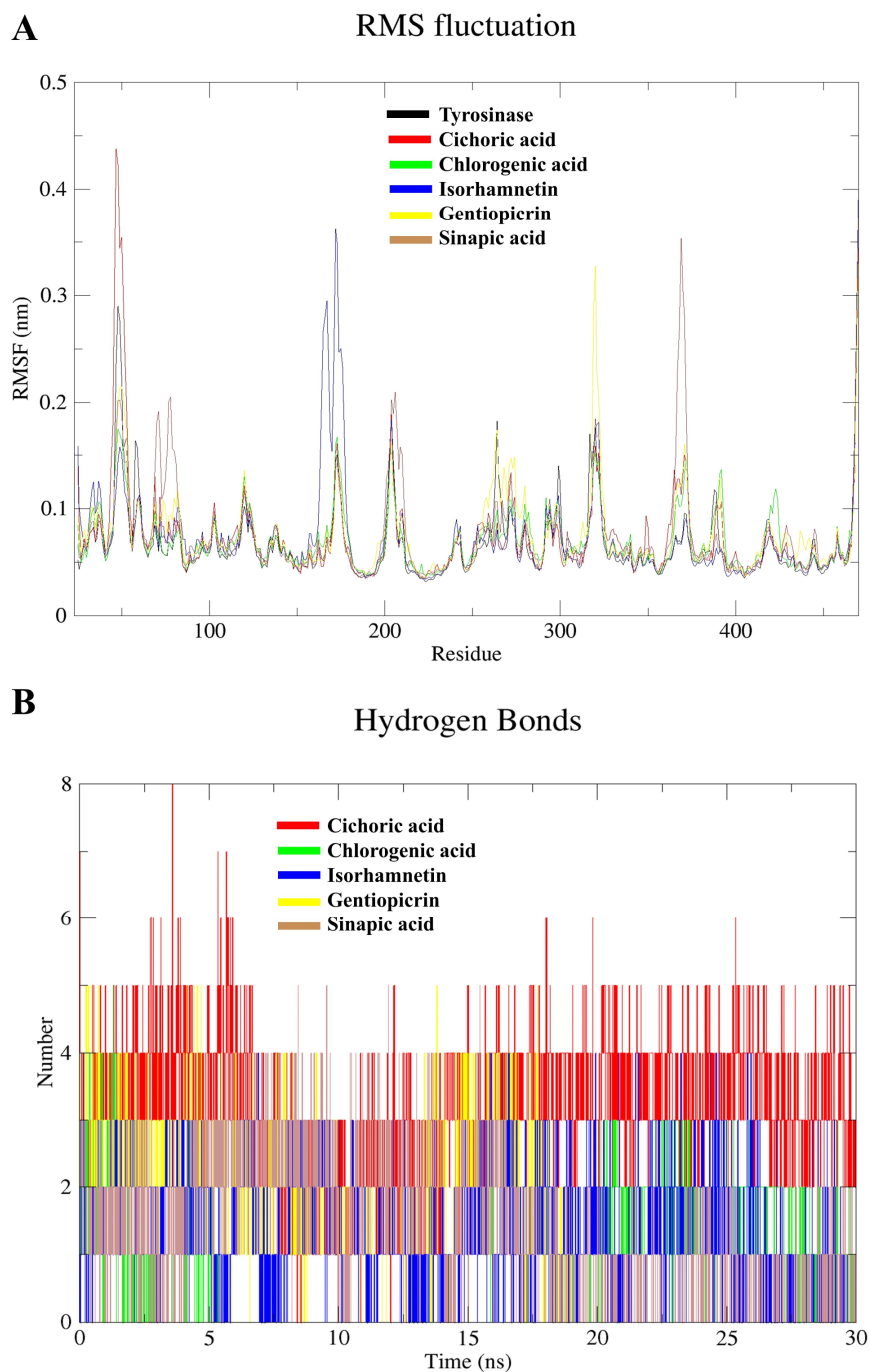
B Hydrogen Bonds

Figure 7. MD simulation (30 ns) analysis of tyrosinase and isolated phytochemicals complexes with tyrosinase; (A) Backbone RMSF per residue number for the free enzyme and the various drug-enzyme complexes and (B) Hydrogen bonding profile of isolated compounds-tyrosinase complexes.
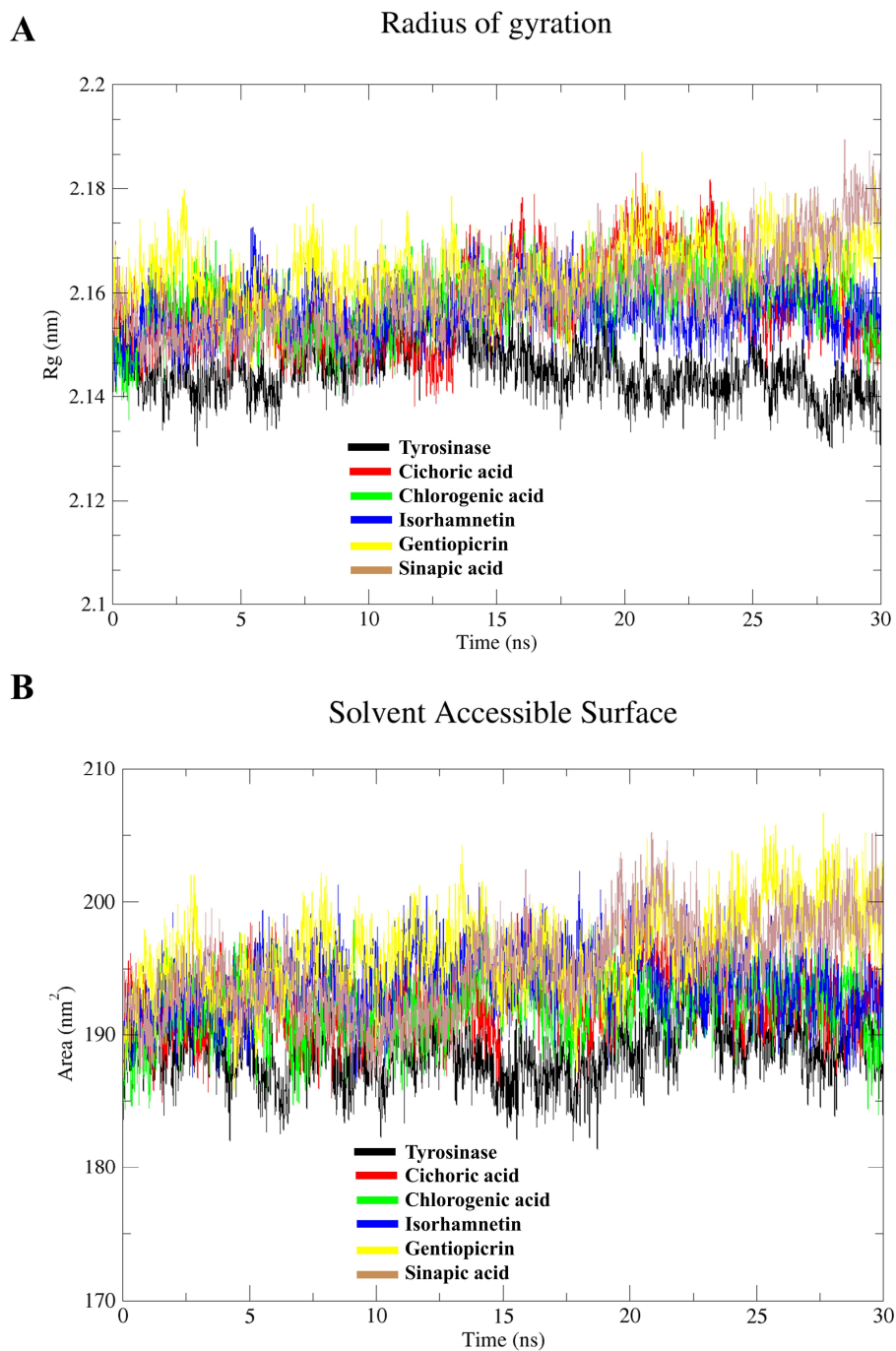
A

Radius of gyration

B

Solvent Accessible Surface

Figure 8. MD simulation (30 ns) analysis of tyrosinase and isolated phytochemicals complexes with tyrosinase; (A) Protein radius of gyration for both free tyrosinase and various drugs-tyrosinase complexes and (B) Protein SASA of the enzyme and various complexes.
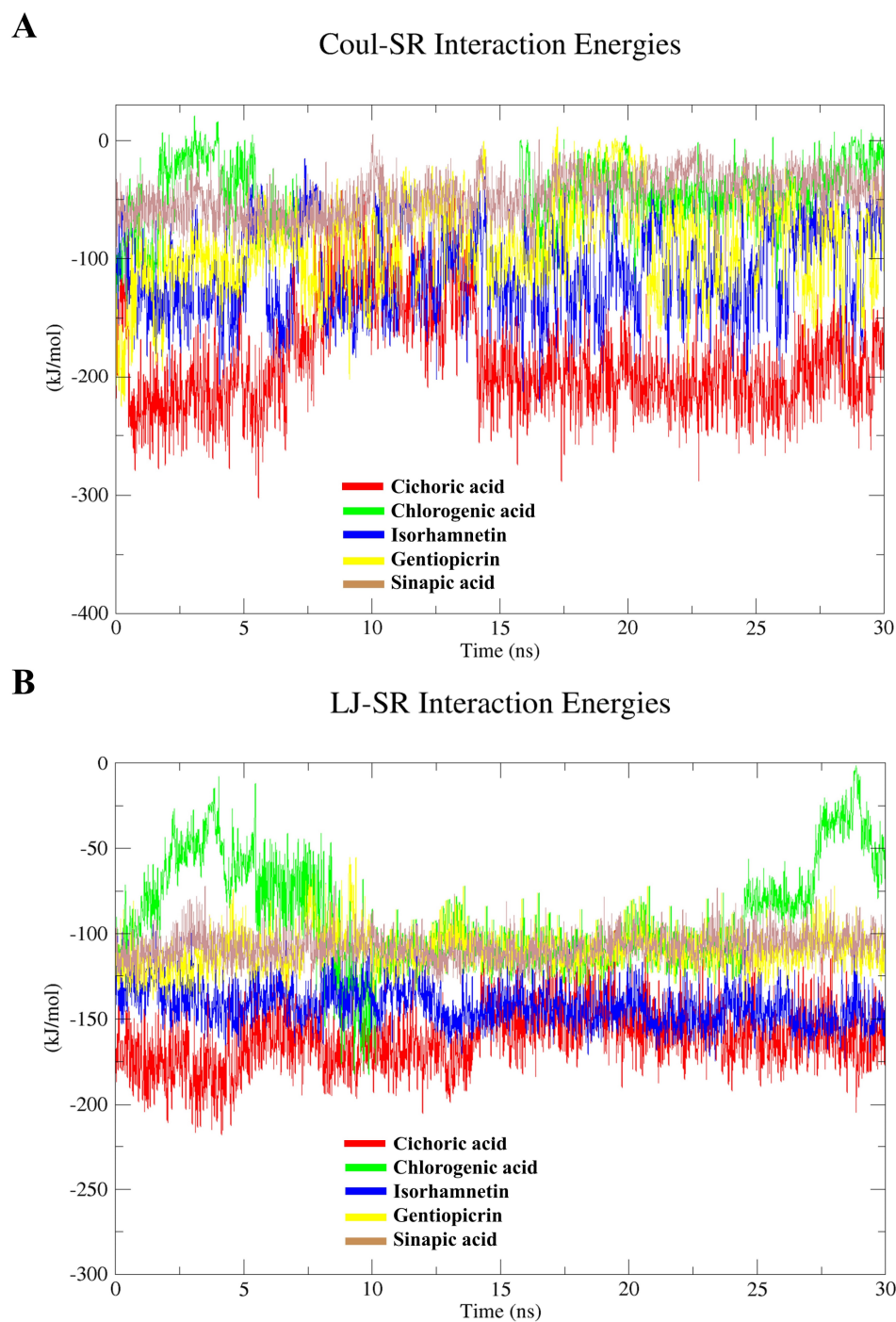
A

Coul-SR Interaction Energies

B

LJ-SR Interaction Energies

Figure 9. MD simulation (30 ns) analysis of tyrosinase and isolated phytochemicals complexes with tyrosinase; (A) Coulomb-SR interactions energies of the enzyme amino acid residues with isolated phenolics and (B) Lennard-Jones-SR interactions energies of the enzyme amino acid residues with isolated phenolics.
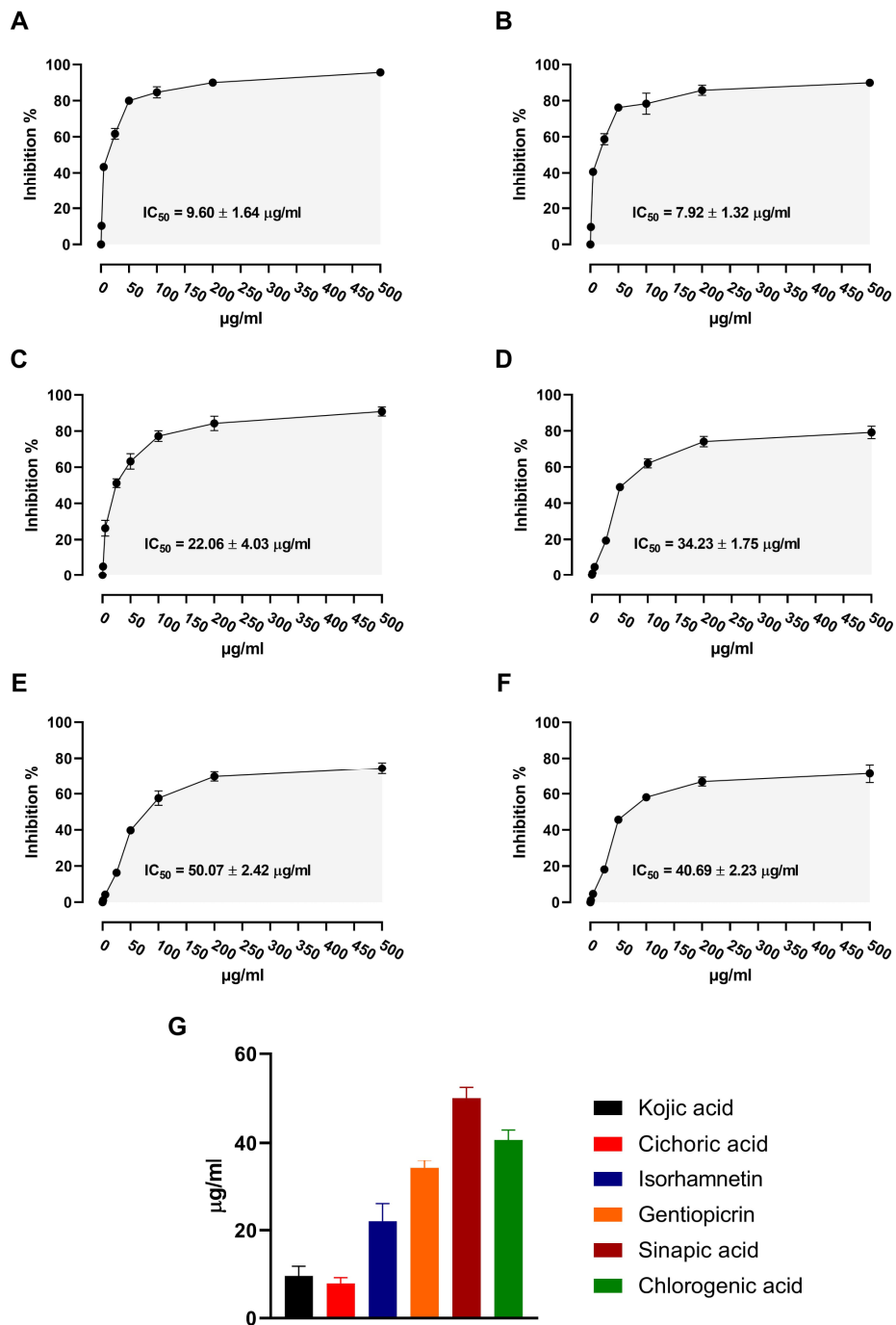
Figure 10. Tyrosinase inhibitory activity of (A) kojic acid, (B) cichoric acid, (C) isorhamnetin, (D) gentiopicrin, (E) sinapic acid, and (F) chlorogenic acid. (G) IC$_{50}$ values of the inhibitory activity of the tested compounds. Data are mean ± SD, N = 3.
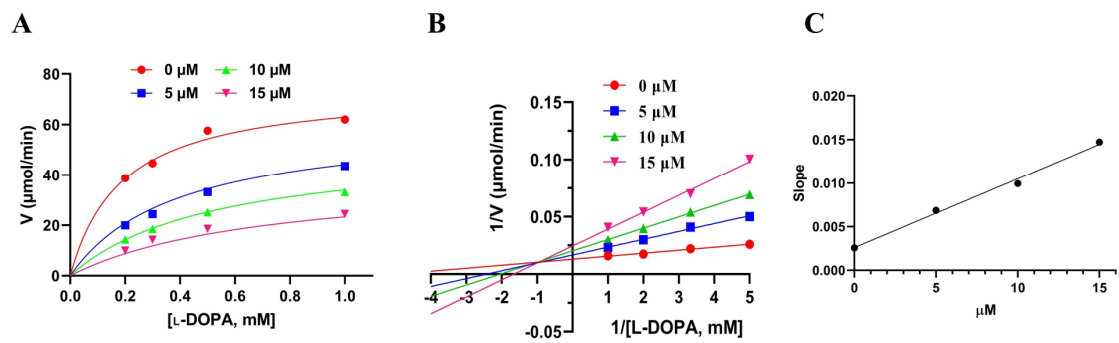
Figure 11. (A) Inhibitory effects cichoric acid on tyrosinase, (B) Lineweaver-Burk plot, and (C) plot of the slope versus concentrations of cichoric acid.